Structure and reactivity of a model catalyst alloy under realistic conditions

2008 J. Phys.: Condens. Matter 20 184018

(http://iopscience.iop.org/0953-8984/20/18/184018)

J. Phys.: Condens. Matter **20** (2008) 184018 (6pp) doi:10.1088/0953-8984/20/18/184018

Structure and reactivity of a model catalyst alloy under realistic conditions

R Westerström[1], J G Wang[2], M D Ackermann[3], J Gustafson[1], A Resta[1], A Mikkelsen[1], J N Andersen[1], E Lundgren[1,6], O Balmes[4], X Torrelles[5], J W M Frenken[3] and B Hammer[2]

[1] Department of Synchrotron Radiation Research, Lund University, Box 118, S-221 00, Sweden
[2] Interdisciplinary Nanoscience Center (iNANO) and Department of Physics and Astronomy, University of Aarhus, DK-8000 Aarhus C, Denmark
[3] Kamerlingh Onnes Laboratory, Leiden University, PO Box 9504, 2300 RA Leiden, The Netherlands
[4] ESRF, 6, rue Jules Horowitz, F-38043 Grenoble cedex, France
[5] Institut the Ciencia de Materials de Barcelona (C.S.I.C.), 08193, Bellaterra, Barcelona, Spain

E-mail: Edvin.lundgren@sljus.lu.se

Received 21 December 2007, in final form 12 March 2008
Published 17 April 2008
Online at stacks.iop.org/JPhysCM/20/184018

Abstract
Using a combined experimental and theoretical approach, we show that a thin RhO_2 oxide film forms on a $Pt_{25}Rh_{75}(100)$ surface at elevated oxygen pressures and temperatures prior to the bulk oxidation. By the use of *in situ* surface x-ray diffraction under realistic CO oxidation reaction conditions, we show that the onset of the growth of thin RhO_2 oxide film coincides with an increase in CO_2 production. During the reaction, the consumed oxide film is continuously re-grown by oxygen in the gas phase. Our theoretical results strongly suggest that the CO adsorbs on the metallic substrate but reacts with the O in the RhO_2 oxide film at the border between the RhO_2 oxide film and the metallic substrate. This scenario could explain the experimental observations of oxidation reactions on other late transition metal surfaces as well as on their corresponding nanoparticles under realistic conditions.

(Some figures in this article are in colour only in the electronic version)

1. Introduction

Frequently, a catalyst is in a different phase from the reactants, e.g. a solid catalyst and gaseous reactants, a situation referred to as heterogeneous catalysis. Information on fundamental processes in heterogeneous catalysis has been a major research field in surface science for decades [1–4].

PtRh alloys can be used as 'three-way' automotive exhaust gas catalysts. They have the ability to simultaneously remove CO, NO_x and hydrocarbons [5, 6], which are all unwanted exhaust gases. A number of adsorbate–surface interaction studies on PtRh surfaces under ultra high vacuum (UHV) conditions have been performed [7, 8]. One of the more important findings is that Pt segregates towards the surface under UHV but that Rh segregates to the surface under oxygen rich conditions, due to the higher affinity to oxygen of Rh than Pt. Under realistic pressures, the behavior of the alloy is in principle unexplored, in particular with regard to the relationship between the structure and the reactivity.

Here we have studied the interaction between a $Pt_{25}Rh_{75}(100)$ alloy surface and O_2 with high resolution core-level spectroscopy (HRCLS), low energy electron diffraction (LEED), scanning tunneling microscopy (STM) and density functional theory (DFT) with the focus on the changes of the surface structure of the alloy. We show that a well ordered thin RhO_2 oxide film distinctly different from the bulk corundum oxide is formed on the $Pt_{25}Rh_{75}(100)$ surface at elevated oxygen pressures and temperatures before the onset of bulk oxidation.

Whereas most traditional electron or ion based surface science techniques are limited to pressures up to a few mbar, surface x-ray diffraction (SXRD) is able to determine structural

[6] Author to whom any correspondence should be addressed.

parameters at surfaces under high pressure operational conditions of several bar. The reason for this highly attractive property is the negligible attenuation due to the low interaction between high energy x-rays and the reactant gas [9–13]. We exploit this property in order to simultaneously probe the surface phases using *in situ* SXRD and CO_2 production using mass spectrometry in a mixture of O_2 and CO at atmospheric pressures and elevated sample temperatures. We show that the onset of the RhO_2 thin film growth coincides with an increase in CO_2 production. Finally DFT calculations provide the atomistic details of the CO_2 production at the surface, identifying a CO oxidation process different from the Mars–van-Krevelen [14] mechanism found on the rutile $RuO_2(110)/Ru(0001)$ surface [15]. Instead, a process involving special sites at the boundaries of surface oxide phases and metal phases is proposed.

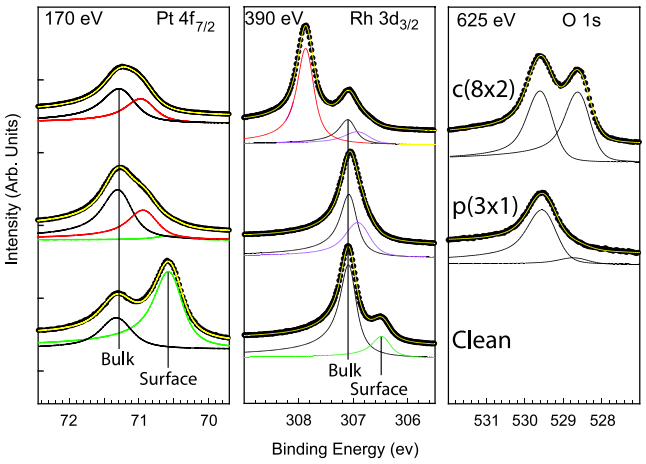

Figure 1. (a) HRCLS from the $Pt_{25}Rh_{75}(100)$ surface with increasing oxygen coverage. Left: Pt $4f_{7/2}$ level. Center: Rh $3d_{3/2}$ level. Right: O 1s level.

2. Experimental and theoretical

The LEED and HRCLS measurements were done using a sample temperature of 90 K at beam line I311 [16] at MAX-lab, Lund, Sweden using a normal emission angle and photon energies of 170, 390 and 625 eV for the Pt $4f_{7/2}$, Rh $3d_{3/2}$ and O 1s levels, respectively.

STM images were recorded in Lund, Sweden, using a commercial Omicron STM1, operated at room temperature. The image shown was recorded in constant current mode. The STM was positioned inside an UHV system with a pressure of 1×10^{-10} mbar.

The SXRD measurements [34] were carried out at the ID3 surface diffraction beamline [17] at the European Synchrotron Radiation Facility (ESRF) using a photon energy of 17 keV. The experimental end-station used contains a batch reaction chamber specifically constructed for studies under high pressures and elevated sample temperatures [18]. The CO gas line is specially equipped with a piece of curled copper tubing which can be heated to 575 K and acts as a trap for Ni carbonyls from the CO gas line. To further clean the CO, the line also has two liquid N_2 traps to clean the CO by subsequent steps of condensation and distillation [19]. The coordinates (H, K, L) in reciprocal space are referred to a basis $(\mathbf{b}_1, \mathbf{b}_2, \mathbf{b}_3)$ with $\mathbf{b}_1$ and $\mathbf{b}_2$ in the surface plane parallel to the $(1\bar{1}0)$ and (110) directions, respectively, and $\mathbf{b}_3$ perpendicular to the surface along (001). Their magnitudes are $|\mathbf{b}_1| = |\mathbf{b}_2| = 2/a$ ($a = a_0/\sqrt{2} = 2.73$ Å) and $|\mathbf{b}_3| = 2/a_0$ ($a_0 = 3.86$ Å bulk lattice constant as calculated from Vegard's rule). The structure factors were calculated by using the software Rod [20].

The $Pt_{25}Rh_{75}(100)$ crystal was cleaned by cycles of Ar^+ sputtering and annealing to 1200 K, followed by oxygen treatment at temperatures up to 1100 K in order to remove residual C and a short anneal in vacuum up to 1300 K in order to remove adsorbed O.

The DFT calculations were performed with the Dacapo-package [21, 22] using ultra soft pseudopotentials for the ions and a plane wave expansion (Ecut = 25 Ryd) for the one-electron wave functions. The revised Perdew, Burke, Ernzerhof (RPBE) functional [21] was used for the exchange–correlation interaction. We investigated a great number of possible $p(3 \times 1)$, $c(8 \times 2)$ chemisorption and trilayer oxide structures while changing the concentration of Pt or Rh in each layer. For the study of chemisorption phases (in either $p(3 \times 1)$ or $c(8 \times 2)$ supercells) four layers of disordered $PtRh_3(100)$ were used, two of which were fully relaxed. For the study of the $c(8 \times 2)$ oxide phase, the trilayer (Rh–O–Rh) was built on top of a three-layer disordered $PtRh_3(100)$ slab and the trilayer and one alloy layer were fully relaxed. The CO oxidation reaction was further investigated on the $p(2 \times 2)$, $p(3 \times 2)$ and $c(8 \times 2)$ chemisorption and oxide phases. The $p(3 \times 2)$—rather than the $p(3 \times 1)$—unit cell was employed in order to model a low CO coverage. In the activity studies for the $c(8 \times 2)$ trilayer oxide an oxide edge was introduced by removal of three RhO_2 units in every supercell. Transition states were located by constrained relaxation.

3. Results and discussion

We first report *ex situ* HRCLS results for the $Pt_{25}Rh_{75}(100)$ surface under UHV conditions before and after oxygen deposition. Figure 1 shows the Pt $4f_{7/2}$, the Rh $3d_{3/2}$ and O 1s core-level spectra. On the clean surface the Pt $4f_{7/2}$ exhibits a bulk and a surface component, their relative intensities being consistent with segregation of Pt to the surface. After a moderate O_2 exposure our STM and LEED results clearly show that the well known $p(3 \times 1)$ adsorption structure [7] is formed. The Pt $4f_{7/2}$ surface component is shifted towards higher binding energies, resulting in a new component at 70.9 eV. The shift reflects that in the $p(3 \times 1)$ structure, the Pt becomes covered by Rh. As the O_2 pressure is increased to 5×10^{-3} mbar using a sample temperature of 700 K, a $c(8 \times 2)$ structure is formed (see figures 2(a)–(c)). The only change that can be observed in the Pt $4f_{7/2}$ spectrum is an overall decrease in intensity. In particular, no intensity at higher binding energies corresponding to Pt atoms in a Pt oxide can be observed, indicating that Pt is not participating in any oxide formation.

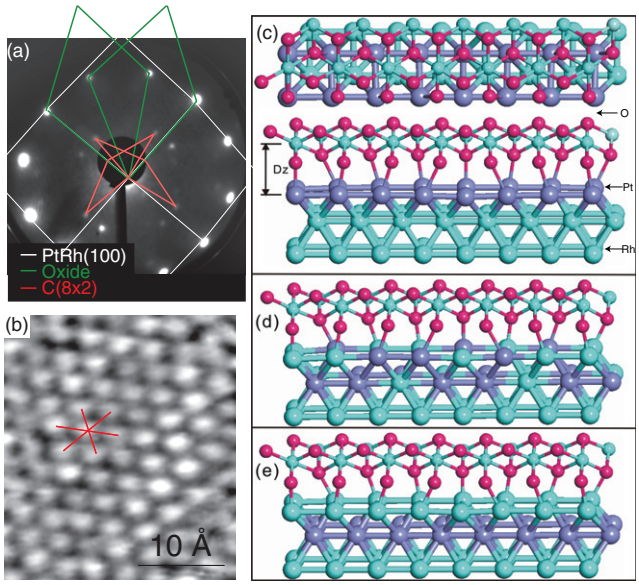

Figure 2. (a) The resulting $c(8 \times 2)$ LEED pattern after an exposure of 5×10^{-3} mbar and a sample temperature of 700 K. Note the two domains. (b) The corresponding STM image (1.8 V, 0.3 nA.) directly revealing the hexagonal structure of the RhO_2 thin film. Structural model as calculated by DFT for the interface layer consisting of (c) only Pt, (d) randomly mixed Pt and Rh, (e) only Rh. The model shown in (c) correspond to the most stable structure. All techniques, including the HRCLS in figure 1, indicate a similar structure for the RhO_2 thin film as found on Rh(111), Rh(110) and Rh(100) [23–26].

Turning to the Rh $3d_{3/2}$ level, the clean spectrum exhibits a relatively weak surface component, indicating that most of the Rh in the surface region is in the second layer before oxygen exposure. As the $p(3 \times 1)$ structure forms, a new component at higher binding energies can be seen at a binding energy of 306.9 eV, which is consistent with Rh atoms coordinated to two O atoms, confirming the $p(3 \times 1)$ chemisorption model [7]. When the $c(8 \times 2)$ structure is formed, the spectrum is dominated by a component at 307.9 eV corresponding to Rh atoms highly coordinated to O. This strongly suggests that the $c(8 \times 2)$ structure is a trilayer O–Rh–O surface oxide (hereafter denoted RhO_2) as has been observed previously on all low-index surfaces of Rh [23–25], which all display a similar shifted Rh $3d_{3/2}$ component. The O 1s level from the $p(3 \times 1)$ structure indicates only one type of oxygen on the surface, consistent with the $p(3 \times 1)$ model [7]. As the O coverage is increased to that of the $c(8 \times 2)$ structure, two components can be observed corresponding to the two different oxygen species in the RhO_2 oxide film. The lower and the higher binding energy components correspond to surface and subsurface oxygen atoms in the trilayer, respectively [23–26]. Furthermore, the LEED and the STM image from the $c(8 \times 2)$ structure shown in figures 2(a) and (b) respectively, can both be explained by a hexagonal RhO_2 overlayer, confirming the HRCLS conclusions. In summary, the HRCLS, LEED and STM measurements of $Pt_{25}Rh_{75}(100)$ concurrently indicate Pt segregation under UHV and the formation of a well ordered ultra-thin RhO_2 surface oxide film at O_2 pressures around 5×10^{-3} mbar using a sample temperature of 700 K. Thin surface oxides have recently also been found for a number of

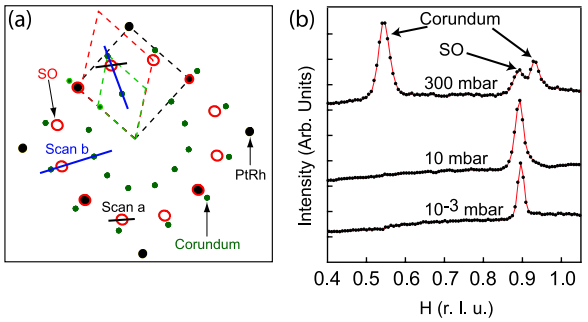

Figure 3. (a) In-plane reciprocal space illustrating the unit cells of the $Pt_{25}Rh_{75}(100)$ (black), the RhO_2 surface oxide (SO) film (red) and the Rh_2O_3 bulk corundum oxide (green). (b) HK-scans (scan b in (a)) for $L = 0.5$ with increasing O pressure.

Pt and Pd surfaces [27–30] as well as on Ag [31, 32], but their role in oxidation catalysis is under debate [33].

The experimental observations are confirmed by DFT calculations. For the clean surface we find a 0.45 eV gain per Pt atom upon segregation of Pt to the surface layer. At an oxygen coverage of 2/3 of a monolayer (ML) in the $p(3 \times 1)$ structure, the segregation reverses and we calculate a 0.62–0.74 eV gain per Pt atom (depending on the local Pt coverage) upon back-segregation of the Pt to the second layer. Finally, increasing the O coverage to 1.8 ML we find strong preference for the formation of the $c(8 \times 2)$ structure depicted in figure 2(c). The DFT calculations show that an interface layer consisting solely of Pt atoms results in the most stable $c(8 \times 2)$ oxide structure (figure 2(c)). The adsorption energy per oxygen is 0.97 eV using the RPBE functional. A random distribution of Pt atoms in both the interface and one bulk layer (figure 2(d)) leads to a decrease of the adsorption energy per oxygen atom by 0.02 eV (0.55 eV potential energy increase for the entire super cell). Finally, the segregation of all Pt atoms into the bulk layer (figure 2(e)) leads to a similar change in the adsorption energy (and to a 0.61 eV increase in the potential energy for the entire supercell). We find good evidence for the calculated structure in figure 2(c) by comparing calculated and measured core-level energies. The calculated shift between the interface Pt atoms and the bulk Pt atoms in the $Pt_{25}Rh_{75}(100)$ crystal is found to be 0.24 eV, in good agreement with the experimental value of 0.34 eV. For the two O atoms enclosing the Rh atoms in the trilayer the calculated shift is 0.85 eV while measurements show a 0.97 eV shift. The distance between the Rh in the trilayer and the Pt at the interface (Dz in figure 2(c)) is calculated to be 3.12 Å while experiments find 2.97 Å (see below). These values can be compared to the corresponding distance in the case of the pure Rh(100) surface [24], which was found to be 2.92 and 2.93 Å by theory and experiment, respectively.

Next we turn to SXRD for *in situ* determination of the surface structures present under different oxygen pressures. A sketch of the in-plane reciprocal space is shown in figure 3(a). Here, the $Pt_{25}Rh_{75}(100)$, the $c(8 \times 2)$ and the corundum $Rh_2O_3(0001)$ bulk oxide reflections and their unit cells are indicated. From the results shown in figure 3(b), we can see that the RhO_2 surface oxide film is covering the surface up to

an oxygen pressure of roughly 10 mbar at 600 K, at which point the Rh_2O_3 corundum bulk oxide starts to form. The out-of-plane scans of the peaks at 300 mbar show that the Rh_2O_3 corundum reflections exhibit bulk-like reflections involving many lattice planes [23], while the RhO_2 surface oxide film reflections display an out-of-plane intensity distribution very similar to the SO structure. This implies a co-existence of the corundum Rh_2O_3 bulk oxide and the RhO_2 surface oxide film on the $Pt_{25}Rh_{75}(100)$ surface under these conditions.

In order to investigate the CO oxidation reactivity of the surface, we may follow simultaneously the phase present at the surface by SXRD and the CO, CO_2 and O_2 partial pressures by the use of a mass spectrometer. Such an experiment is shown in figure 4(a), where the lower part shows scans according to scan a in figure 3(a), while the upper part shows the partial pressures detected in the mass spectrometer. In this experiment, the PtRh surface was initially exposed to 500 mbar of oxygen at 500 K, and a number of reduction and oxidation cycles were observed. At time 0, the surface oxide peak can clearly be observed. By introducing 200 mbar of CO ($t = 1750$ s), the surface oxide is removed, as evidenced by the disappearance of the diffraction peak. As the CO is consumed by the oxidation into CO_2 in the batch reactor, the CO/O partial pressure ratio is continuously reduced, since two CO molecules are consumed by one O_2 molecule. When the CO pressure is sufficiently low, the surface re-oxidizes ($t = 4600$ s), which can be seen by the reappearance of the diffraction signal from the surface oxide (red intensity envelope). At exactly the same time, the CO oxidation rate is increasing, as deduced from the measured partial pressures.

A second experiment is shown in figure 4(b), in which we scan according to scan b in figure 3(a), in order to probe the bulk and surface oxides simultaneously. In this experiment, we first exposed the surface to 250 mbar of O_2 using a sample temperature of 500 K. The resulting surface was observed to be very similar to the one identified in figure 3(b) (upper scan), a co-existence of the bulk Rh_2O_3 oxide and the RhO_2 surface oxide film. Introducing 61 mbar of CO (not shown) removed the RhO_2 surface oxide film peaks but the Rh_2O_3 corundum peaks remained. As the CO is consumed and the CO pressure is sufficiently low, the surface re-oxidizes ($t = 1125$ s), which can be seen by the reappearance of the diffraction signal from the RhO_2 surface oxide film (red intensity envelope). At exactly the same time, the CO oxidation rate increases, as deduced from the kink in the measured partial pressure (blue curve). The out-of-plane diffraction from the reappearing surface oxide film was measured during the reaction and is shown in figure 4(c). Using the DFT model (figure 2(c)) of the surface oxide to calculate the diffracted intensities, a comparison between experimental and calculated structure factors shown in figure 4(c) shows that it is indeed the surface oxide reappearing on the surface. The measurements indicate a 5% inward relaxation of the height, Dz, of the Rh layer in the trilayer O–Rh–O towards the bulk, as compared to the DFT model. Our observations lead us directly to conclude that, under these conditions, the phase of the alloy surface in which the RhO_2 surface oxide film is present is more active for CO oxidation than phases of the alloy surface in which either the

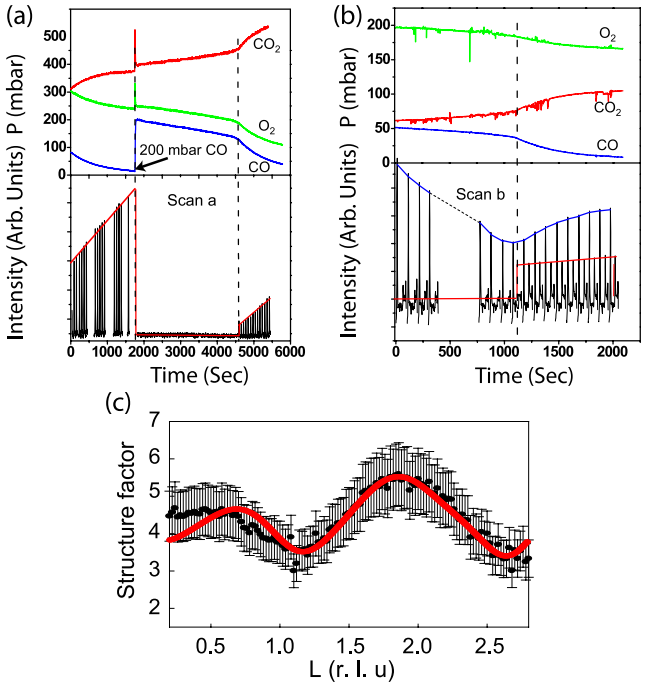

Figure 4. (a) Repetitive HK-scans (scan a in figure 3(a)) during reaction conditions (bottom part) with simultaneous mass spectroscopy measurements of the gas content (top part). The red intensity envelope indicates the surface oxide diffraction peak. (b) Repetitive HK-scans (scan b in figure 3(a)) during reaction conditions (bottom part) with simultaneous mass spectroscopy measurements of the gas content (top part). The blue and red intensity envelopes indicate the bulk and the surface oxide diffraction peaks, respectively. (c) Measured (black dots) and calculated (red line) out-of-plane structure factors from the surface oxide during the high activity branch, revealing that the appearance of the RhO_2 oxide film on the surface is responsible for the increase in the reaction rate.

corundum Rh_2O_3 bulk oxide or the metal alloy surface on the $Pt_{25}Rh_{75}(100)$ surface is dominant.

Previously, the rate of production of CO_2 on Rh has been observed to decrease at very high O_2 partial pressures which have been related to a poisoning effect due to bulk oxide formation [35]. Our measurements confirm this observation; however, they also demonstrate that the presence of a thin RhO_2 surface oxide film on the $Pt_{25}Rh_{75}(100)$ surface is responsible for a large increase in the detected CO_2 signal.

We have previously shown that under UHV conditions, CO cannot adsorb on a RhO_2 surface oxide film [36], due to the oxygen-terminated surface yielding no available sites for the CO to adsorb onto. This observation is confirmed by the present DFT calculations. However, the RhO_2 surface oxide film can still readily be reduced, and the reason could be related to sites at the edge between the RhO_2 oxide islands and the metal surface [36].

Our calculations support this assertion. The CO oxidation process, $O(a) + CO(a) \rightarrow CO_2(g)$, calculated for a $Pt_{25}Rh_{75}(100)$ surface covered with either a fictional $p(2 \times 2)$ or the real $p(3 \times 1)$ chemisorbed oxygen structure yields relatively high energy barriers of 0.76 and 0.72 eV, respectively (see figures 5(a) and (b)). On the contrary, the reaction process involving the edge of a RhO_2 surface oxide island and an

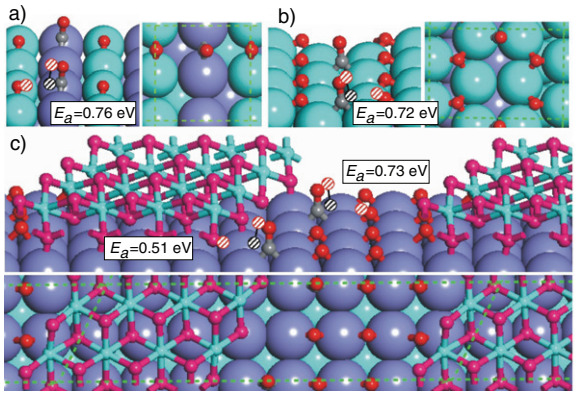

Figure 5. DFT based structures and CO oxidation energy barriers (E_a) for (a) $p(2 \times 2)$ phase, (b) $p(3 \times 1)$ phase and (c) border between the $c(8 \times 2)$ (RhO_2 surface oxide film) and the oxygen covered metal surface. Gray, red, green and blue spheres represent C, O, Rh and Pt atoms, respectively. Hatched circles illustrate the transition states for the CO oxidation.

oxygen covered metal surface, as shown in figure 5(c), yields an energy barrier of 0.51 eV, explaining the experimentally detected increase in CO_2 production as this surface oxide appears.

Based upon the present results, the high reactivity of the $Pt_{25}Rh_{75}(100)$ surface for CO oxidation in a realistic environment can be explained as follows. On the RhO_2 surface, the adsorption energy for CO is 0.36 eV (exothermic), which does not counteract the $-$TS free energy term of gas phase CO at normal temperatures and pressures meaning that CO cannot adsorb on pure oxide surfaces. On the pure metallic CO binds by 0.95 eV (exothermic), i.e. much more strongly, but the energy barrier for a reaction between chemisorbed O and CO molecules forming CO_2 is too high to promote CO oxidation. However, on the border between the RhO_2 surface oxide film and the metallic surface, the energy barrier formation for CO_2 is lowered and each phase, the surface oxide and the metallic surface, is capable of holding one reactant each in large quantities ensuring a high reaction probability. In our batch reactor, the surface oxide film undergoes decomposition by the removal of oxygen atoms, but in a flow reactor steady state conditions may be achieved such that the surface oxide film is replenished during the reaction. If steady state is not achieved, the result might be that of spatial and temporal oscillations [37–39].

The scenario presented here is likely to explain observations from small Rh nanoparticles; a Rh phase similar to Rh_2O_3 was found to be a highly effective catalyst which also displayed the lowest light-off temperature [40]. Similar scenarios could also explain recent observations on Pt, Pd and Rh single crystal model catalysts [41–46] under certain conditions. It should be noted that the $Pt_{25}Rh_{75}(100)$ surface is much more difficult to oxidize than a pure Rh(100) surface, the difference being a factor of 1000 in pressure in order to form the surface oxide. No bulk diffusion of either Rh or Pt atoms occurs at the sample temperatures used in the present investigation, inhibiting bulk oxide formation due to a depletion of Rh in the near-surface region. The result could be the formation of a thinner, and also more reactive, surface oxide layer on the alloy as compared to on the pure metal surface.

4. Summary

In summary, we have studied the oxidation of a $Pt_{25}Rh_{75}(100)$ alloy using traditional electron based surface science techniques up to a pressure of 5×10^{-3} mbar. The experimental data show that under UHV conditions, Pt segregates to the surface, while Rh segregates when oxygen is introduced into the UHV chamber. Further, our experiments show that a thin trilayer RhO_2 surface oxide film is formed at an O_2 pressure of 5×10^{-3} mbar, which has been found on all Rh surface orientations investigated so far. DFT calculations support the experimental findings. By the use of *in situ* SXRD, the oxidation at higher pressure could be followed in a batch reactor, revealing the formation of the corundum $Rh_2O_3(0001)$ bulk oxide. Having identified all the relevant reflections in reciprocal space, the CO oxidation at realistic conditions could be followed by *in situ* SXRD and mass spectrometry. The experiments showed that while the bulk oxide had no or little impact on CO_2 production, the appearance of the trilayer RhO_2 surface oxide film coincided with a substantial increase in the rate of production of CO_2. A thorough theoretical evaluation of a number of processes and their energetics supports a model in which the CO oxidation reaction occurs at the border between the surface oxide and the metallic surface.

Acknowledgments

This work was supported by the Swedish Research Council, the Crafoord foundation, the Knut and Alice Wallenberg foundation, the Spanish MCyT (MAT2002-02808), the Danish Research Council, Dansk Center for Scientific Computing, the European Union under Contract No. NMP3-CT-2003-505670 (NANO2). Support by the MAX-lab and ESRF staff is gratefully acknowledged.

References

[1] Somorjai G A 1994 *Introduction to Surface Chemistry and Catalysis* (New York: Wiley)
[2] Ertl G, Knözinger H and Weitkamp J 1997 *Handbook of Heterogeneous Catalysis* (New York: Wiley)
[3] Nieuwenhuys B E 2000 *Adv. Catal.* **44** 259
[4] Zaera F 2001 *Prog. Surf. Sci.* **69** 1
[5] Taylor K C 1984 *Automobile Catalytic Converters* (Springer: Berlin)
[6] Shelef M and Graham G W 1994 *Catal. Rev. Sci. Eng.* **36** 433
[7] Sporn M, Platzgummer E, Gruber E L D, Schmid M, Hofer W and Varga P 1998 *Surf. Sci.* **416** 384
[8] Baraldi A *et al* 2005 *J. Am. Chem. Soc.* **127** 5671
[9] Lundgren E, Gustafson J, Mikkelsen A, Andersen J N, Stierle A, Dosch H, Todorova M, Rogal J, Reuter K and Scheffler M 2004 *Phys. Rev. Lett.* **92** 046101
[10] Stierle A, Kasper N, Dosch H, Gustafson J, Mikkelsen A, Andersen J N and Lundgren E 2005 *J. Chem. Phys.* B **122** 44706
[11] He Y B, Knapp M, Lundgren E and Over H 2005 *J. Phys. Chem.* B **109** 21825

[12] Westerström R *et al* 2007 *Phys. Rev.* B **76** 155410
[13] Ackermann M D *et al* 2005 *Phys. Rev. Lett.* **95** 255505
[14] Mars P and van Krevelen D W 1954 *Chem. Eng. Sci.* **3** 41
[15] Over H, Kim Y D, Seitsonen A P, Wendt S, Lundgren E, Schmid M, Varga P, Morgante A and Ertl G 2000 *Science* **287** 1474
[16] Nyholm R, Andersen J N, Johansson U, Jensen B N and Lindau I 2001 *Nucl. Instrum. Methods Phys. Res.* A **467** 520
[17] Ferrer S and Comin F 1995 *Rev. Sci. Instrum.* **66** 1674
[18] Bernard P, Peters K, Alvarez J and Ferrer S 1992 *Rep. Prog. Phys.* **55** 599
[19] Ackermann M D 2007 *PhD Thesis* Kamerlingh Onnes Laboratory, Leiden University, PO Box 9504, 2300 RA Leiden, The Netherlands
[20] Vlieg E 2000 *J. Appl. Crystallogr.* **33** 401
[21] Hammer B, Hansen L B and Nørskov J K 1999 *Phys. Rev.* B **59** 7413
[22] http://www.camp.dtu.dk/campos
[23] Gustafson J *et al* 2004 *Phys. Rev. Lett.* **92** 46101
[24] Gustafson J *et al* 2005 *Phys. Rev.* B **71** 115442
[25] Dri C, Africh C, Esch F, Comelli G, Dubay O, Köhler L, Mittendorfer F, Kresse G, Dudin P and Kiskinova M 2006 *J. Chem. Phys.* **125** 094701
[26] Lundgren E, Mikkelsen A, Andersen J N, Kresse G, Schmid M and Varga P 2006 *J. Phys.: Condens. Matter* **18** R481
[27] Lundgren E, Kresse G, Klein C, Borg M, Andersen J N, De Santis M, Gauthier Y, Konvicka C, Schmid M and Varga P 2002 *Phys. Rev. Lett.* **88** 246103
[28] Todorova M *et al* 2003 *Surf. Sci.* **541** 101
[29] Kostelnik P, Seriani N, Kresse G, Mikkelsen A, Lundgren E, Blum V, Sikola T, Varga P and Schmid M 2007 *Surf. Sci.* **601** 1574
[30] Li W X, Österlund L, Vestergaard E K, Vang R T, Matthiesen J, Pedersen T M, Lægsgaard E, Hammer B and Besenbacher F 2004 *Phys. Rev. Lett.* **93** 146104
[31] Schmid M *et al* 2006 *Phys. Rev. Lett.* **96** 146102
[32] Schnadt J, Michaelides A, Knudsen J, Vang R T, Reuter K, Lægsgaard E, Scheffler M and Besenbacher F 2006 *Phys. Rev. Lett.* **96** 146101
[33] Rupprechter G and Weilach C 2007 *Nano Today* **2** 20
[34] Robinson I K and Tweet D J 1992 *Rep. Prog. Phys.* **55** 599
[35] Peden C H F, Goodman D W, Blair D S, Berlowitz P J, Fischer G B and Oh S H 1988 *J. Phys. Chem.* **92** 1563
[36] Lundgren E *et al* 2005 *J. Electron Spectrosc. Relat. Phenom.* **144** 367
[37] Turner J E, Sales B C and Maple M B 1981 *Surf. Sci.* **103** 54
[38] Ertl G, Norton P R and Rstig J 1982 *Phys. Rev. Lett.* **49** 177
[39] Gruyters M and King D A 1997 *J. Chem. Soc. Faraday Trans.* **93** 2947
[40] Newton M A, Dent A J, Diaz-Moreno S, Fiddy S G, Jyoti B and Evans J 2006 *Chem. Eur. J.* **12** 1975
[41] Hendriksen B L M and Frenken J W M 2002 *Phys. Rev. Lett.* **89** 046101
[42] Hendriksen B L M and Frenken J W M 2004 *Surf. Sci.* **552** 229
[43] Wang J G *et al* 2005 *Phys. Rev. Lett.* **95** 256102
[44] Li W X and Hammer B 2005 *Chem. Phys. Lett.* **409** 1
[45] Rogal J, Reuter K and Scheffler M 2007 *Phys. Rev. Lett.* **98** 1 046101
[46] Chen M S, Cai Y, Yan Z, Gath K K, Axnanda S and Goodman D W 2007 *Surf. Sci.* **601** 5326